Available online at www.sciencedirect.com
ScienceDirect
Journal of Nuclear Materials 356 (2006) 78–87
journal of nuclear materials
www.elsevier.com/locate/jnucmat

Bending tests on T91 samples implanted with 0.25 at.% helium: Experiments and mechanical analysis

J. Henry [a,*], L. Vincent [a], X. Averty [b], B. Marini [a], P. Jung [c]

[a] CEA Saclay, DEN/DMN/SRMA, F-91191 Gif-sur-Yvette cedex, France
[b] CEA Saclay, SEMI, F-91191 Gif-sur-Yvette cedex, France
[c] Institut für Festkörperforschung, Forschungszentrum Jülich, D-52425 Jülich, Germany

Abstract

In order to investigate helium effects on the fracture properties of martensitic mod 9Cr–1Mo (T91) steel, miniature Charpy specimens were implanted at 250 °C in the notch region to 0.25 at.% helium using a degraded 34 MeV ^{3}He ion beam and subsequently submitted to static bending tests at room temperature. For the six implanted specimens, a 'pop-in' phenomenon, which is an arrested unstable crack extension, was systematically recorded during testing. In the implanted zones of the samples, the fracture mode was fully brittle with both intergranular and cleavage fracture, whereas for unimplanted samples tested at −170 °C, the fracture mode was found to be 100% cleavage. Finite element simulations of the tests performed on unimplanted and implanted specimens were also carried out to determine stress and strain fields at the onset of crack propagation. Based on these computations, the fracture toughness of implanted T91 was tentatively evaluated using the Beremin model of the local approach to brittle fracture.

1. Introduction

Tempered 9Cr martensitic steels are candidate structural materials for fusion reactors and spallation neutron sources. Indeed, these steels have high strength up to temperatures around 500 °C, low thermal stresses and good resistance to high dose fission neutron irradiation at temperatures above 400 °C. For instance, modified 9Cr–1Mo martensitic steel (referred to in the following using the commercial denomination 'T91') was used to manufacture the lower liquid metal container (i.e. the proton beam window) of the MEGAPIE spallation target [1].

However, an important issue as regards the use of tempered 9Cr martensitic steels in fusion and spallation devices is the helium induced embrittlement. While it has been well established that martensitic steels are relatively immune to the so-called 'high temperature' helium embrittlement phenomenon (see for instance [2]), helium effects at low temperature are still a matter of controversy. It was recently shown [3,4] that implanted helium can induce a drastic degradation of the tensile properties of 9Cr–1Mo steels. Following implantation of

* Corresponding author. Tel.: +33 1 69088508; fax: +33 1 69087130.
E-mail address: jean.henry@cea.fr (J. Henry).

0022-3115/$ - see front matter © 2006 Elsevier B.V. All rights reserved.
doi:10.1016/j.jnucmat.2006.05.004

0.5 at.% helium at 250 °C, a complete ductility loss was observed, associated with an intergranular fracture mode. Some ductility was retained in the specimens implanted with 0.25 at.% helium. However, for tensile tests performed on thin specimens, the stress triaxiality ratio is low. It may well be that the helium concentration threshold for complete ductility loss would be lower if measured using mechanical tests characterized by higher values of the triaxiality ratio. Indeed, high stress triaxiality promotes brittle fracture modes such as cleavage and intergranular fracture. A number of experimental studies have previously been performed with the aim of characterizing helium effects on the fracture properties of martensitic steels. Most of these studies have used the doping technique, with either nickel or boron isotopes, which allows to produce helium in bulk specimens via transmutation reactions with thermal neutrons. However, the clear demonstration of a specific helium effect is difficult, because of a number of artefacts induced by the doping (modifications of transformation temperatures by nickel, formation of nickel rich precipitates during irradiation, boron segregation to grain boundaries and formation of Li as well as helium etc.) as discussed in detail in [5,6]. The helium implantation technique was also used, for instance by Lindau et al. [7] and Kasada et al. [8]. Lindau et al. implanted F82H (a reduced activation 8Cr2WVTa martensitic steel) miniature Charpy specimens at 250 °C using a degraded 104 MeV alpha particle beam. The total helium concentration was 300 appm He and the corresponding displacement damage 0.2 dpa. Impact tests were carried out, and the ductile-to-brittle transition temperature (DBTT) shift was compared to that measured following neutron irradiation at 250 °C to 0.2 dpa and very low helium production (8 appm). The shift after neutron irradiation was 18 °C, while a 42 °C shift was found following implantation. This difference was attributed to an embrittling effect of helium.

Moreover, homogeneous helium implantation of 0.2 mm thick 9Cr–1W miniature disks using 36 MeV alpha particles was carried out by Kasada et al. at temperatures in the range 80–150 °C to a maximum helium content of 580 appm (0.23 dpa). The DBTT shift was evaluated based on Small Punch tests. When plotted against irradiation hardening and compared to DBTT shifts measured after neutron irradiation with negligible helium production, the measured shift was within the trend of the neutron irradiation data. The authors thus concluded that there was essentially no effect of helium on the embrittlement. Dai and co-workers also conducted small punch tests on miniatures disks (T91 and other martensitic steels) irradiated in a spallation environment at temperatures between 90 and 275 °C up to a maximum dose of 9.4 dpa generating about 770 appm He [9,10]. They reported an almost linear correlation between the DBTT shift and the helium content in the specimens.

Finally, Odette et al. [5] have analyzed the relation between the irradiation/implantation induced hardening $\Delta\sigma_y$ and the DBTT shift ΔT, using a variety of published data. Based on their analysis, they conclude that up to concentrations of several hundred appm, helium plays a minor role on fast fracture of tempered martensitic steels. However, the authors add that at higher helium contents, the increase of the $c = \Delta T/\Delta\sigma_y$ ratio is an indication that non-hardening helium embrittlement (NHHE) is probably occurring.

Obviously, there is a need to better characterize and progress in the understanding of the intrinsic effects of helium on the fracture properties of 9Cr martensitic steels. To this end, three-point bending tests were carried out on helium implanted specimens and tests results were analyzed using finite elements calculations. In addition, bending tests were performed on pristine T91 at low temperature. The goal was to compare the fracture properties of T91 loaded with helium to those of unimplanted T91 in the brittle domain.

2. Experimental

2.1. Materials and specimens

The T91 heat used in this study had the composition shown in Table 1. Miniature Charpy, toughness and tensile specimens were machined from a 15 mm thick plate, which was in the normalized and tempered metallurgical condition (solution annealed for 1 h at 1040 °C, fast cooled, reheated 1 h at 760 °C and fast cooled). The miniature Charpy specimens (KLST geometry, see Fig. 1) were cut with TL orientation. The notch root radius

Table 1
Composition of the T91 steel (in wt%)

C	Cr	Mo	V	Nb	Ni	Mn	N	P	Si
0.1	8.73	0.99	0.19	0.031	0.23	0.43	0.029	0.021	0.32

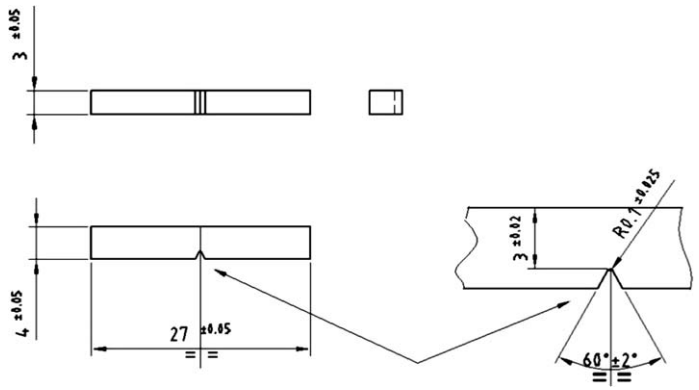

Fig. 1. Dimensions (in mm) of the miniature KLST Charpy specimens. Note that for the helium implanted specimens the root notch radius value was 60 μm.

was 100 μm, i.e. the usual value, for the specimens which were used for bending tests at low temperature. In the case of the specimens dedicated to helium implantation experiments, the notch radius was 60 μm, in order to ensure that failure initiation would take place well within the implanted zones of the specimens (cf. Section 2.2). The geometries of the specimens used for the measurements of tensile and toughness properties at low temperature are depicted in Figs. 2 and 3, respectively.

2.2. Implantation

The implantations were carried out using the compact cyclotron of Forschungszentrum Jülich. The experimental set-up for the implantation of tensile specimens was detailed in [3]. For the present experiments, implantation was performed with a ^{3}He ion beam of 34 MeV energy (behind a 25 μm Hasteloy window), which was degraded by a wheel with 24 aluminium foils of appropriate thicknesses.

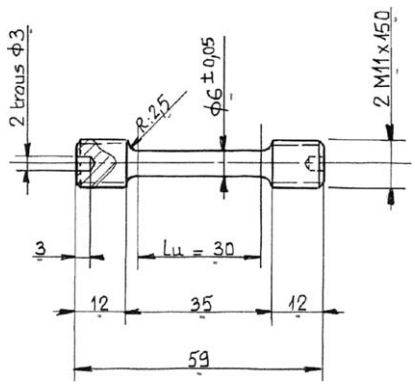

Fig. 2. Dimensions (in mm) of the cylindrical tensile specimens.

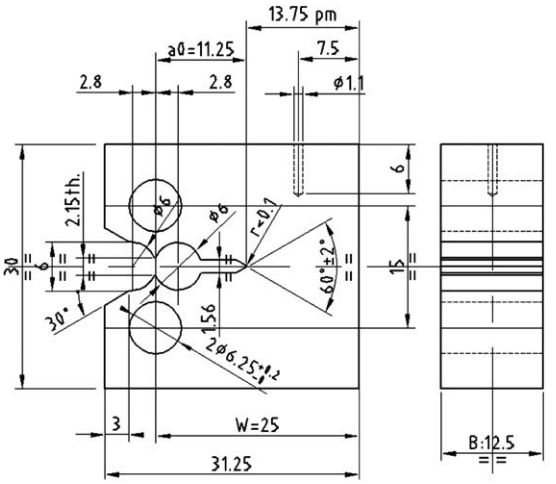

Fig. 3. Dimensions (in mm) of the Compact Tension (CT) specimens.

Three Charpy specimens were mounted on top of each other with mutual distances of 0.5 mm and clamped at both ends by a slight pressure from a small bolt. The beam area of 13 × 4 mm was centred on the notches. As a result, the T91 specimens were implanted homogeneously with helium up to a depth equal to the range of the 34 MeV ^{3}He particles, i.e. 240 μm. The specimens were heated by the beam current, while cooling was supplied by flowing helium gas. The gas flow rate allowed to adjust the implantation temperature. Due to the thickness (4 mm) of the Charpy specimens and the limited range of the bombarding particles, a significant temperature gradient exists between the irradiated frontside and the backside, where pyrometer measurements are taken. The results of finite element calculations (FEM) for the temperature differences

between front (T_1) and backside (T_2) can be summarised by

$$(T_1 - T_2)/P = 5.12 - 3.8 \times 10^{-4}\alpha, \quad (1)$$

where α (W/m^2/K) is the heat-transfer coefficient and P (W) is the beam power on the target. A value of 25 W/mK for the T91 thermal conductivity was used. P is obtained from

$$P = Z^{-1} j E_{\max}/2, \quad (2)$$

where Z is the charge of the particles (2 for He), j (A) the beam current on one specimen ($\approx$1.2 μA), and $E_{\max}$ (eV) the maximum energy of the degraded beam (34×10^6). According to the FEM result, α is related to T_1 by

$$T_1\ (^\circ\mathrm{C}) = T_0 + 320P/\sqrt{\alpha}, \quad (3)$$

where T_0 (°C) is the temperature of the cooling gas ($\approx$25). Eqs. (1)–(3) give then the following expression for T_2 (°C):

$$T_2 = T_1 - P(5.12 - 0.1216P/(T_1 - 25)). \quad (4)$$

For the present experiments for which the nominal implantation temperature was 250 °C (T_1) and beam powers of about 10 W, the second terms in Eqs. (1) and (4) can be neglected, so that

$$T_2 = T_1 - 5.12P. \quad (5)$$

For $P = 10$ W, the linear temperature gradient from front to back amounts to about 50 °C/4 mm. FEM-elements with a thickness of about 400 μm at the backside of the specimens and of 240 μm at the frontside were used, with homogeneous energy deposition across the first element in the implanted area. Therefore no temperature distribution was modelled over the implanted depth, but a temperature difference of about 3 °C can be estimated, with the maximum at the inner side.

Six Charpy specimens were implanted at 250 °C up to a concentration of 0.25 at.% He and subsequently shipped to CEA Saclay.

2.3. Mechanical tests

Three-point bending tests on helium implanted specimens were carried out in a glove box located in the Saclay hot laboratory, since the samples had been activated as a result of implantation. The tests were conducted at room temperature in crosshead displacement control mode at a crosshead speed of 0.1 mm/mn. The testing machine was equipped with a high frequency data acquisition system in order to allow the detection of possible 'pop-in' phenomena inside the implanted zone below the notch.

Tensile, toughness and three-point bending tests were carried out at −170 °C on unimplanted specimens. The tests were conducted using a servo-hydraulic machine in a conventional laboratory. The specimens were brought down to −170 °C in a chamber mounted around the specimens and acclimatized for about 30 min prior to testing. For the three-point bending tests, the same procedure as that described above was used. The tensile tests were carried out with a strain rate of about 4×10^{-4} s^{-1}. The fracture toughness tests were performed in accordance with the ISO12737 standard. The specimens were first pre-cracked by fatigue. Following testing, the specimens were heat tinted and broken by fatigue in order to measure the pre-crack shape and length.

3. Results

3.1. Unimplanted T91: bending and toughness tests at low temperature

Three-point bending tests were performed on 13 miniature Charpy specimens. Values of the opening displacement at failure were measured and used to compute the experimental failure probability, p_r, according to the following equation:

$$p_r = (i - 0.5)/N, \quad (6)$$

where N is the total number of tests and i the rank of a given experiment. The experiments were ranked from 1 to N based on increasing opening displacement at failure.

The obtained failure probability values are plotted in Fig. 4. Likewise, toughness tests were carried out on four CT specimens at −170 °C and the results were used to derive the experimental failure probability, which is presented in Fig. 5. In addition, scanning electron microscopy (SEM) examinations of fracture surfaces were performed on six broken miniature Charpy specimens. As expected, the failure mode was predominantly brittle cleavage, as shown in Fig. 6. However, on some specimens, small zones with intergranular fracture appearance were also detected.

3.2. He-implanted T91: bending tests at room temperature

Static bending tests were carried out at room temperature on six miniature Charpy specimens

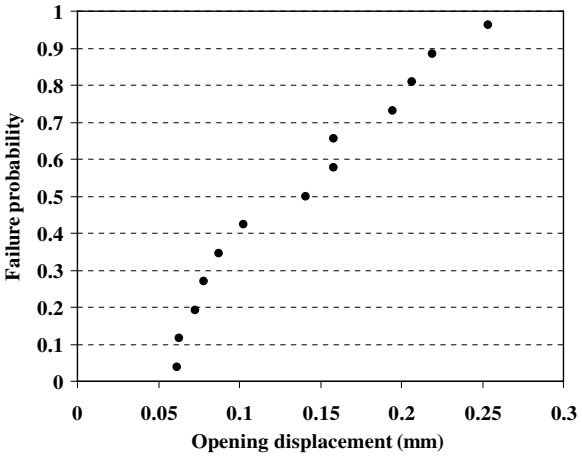

Fig. 4. Failure probability as a function of opening displacement for T91 submitted to three-point bending tests at −170 °C.

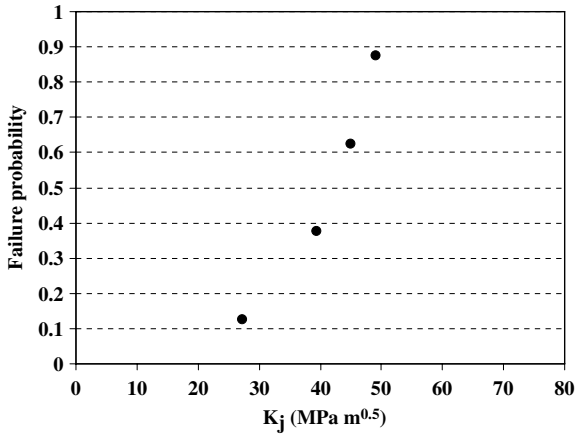

Fig. 5. Failure probability as a function of stress intensity factor for T91 CT specimens tested at −170 °C.

implanted in the notch region with 0.25 at.% helium. In all cases, a 'pop-in' phenomenon was

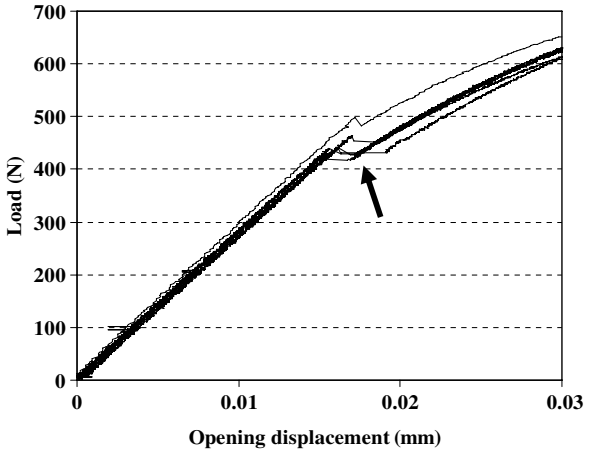

Fig. 7. Applied load as a function of opening displacement for T91 implanted at 250 °C in the notch with 0.25 at.% He and tested in three-point bending at room temperature. For all specimens, a 'pop-in' (indicated by the arrow) occurred during testing.

recorded (see Fig. 7), at an applied load in the range 400–500 N. This phenomenon is due to brittle crack initiation and propagation in the implanted zone below the notch, followed by crack arrest in the tough unimplanted material, as clearly demonstrated by SEM examinations carried out on two broken specimens. Representative micrographs are presented in Fig. 8. The fracture surfaces consist of two zones: the first one, located just below the notch, has a fully brittle appearance. In this zone, the fracture mode was both cleavage (Fig. 8(b)), and intergranular fracture (Fig. 8(c)). The brittle region corresponds to the implanted zone since its depth below the notch exactly matches the alpha particle range, i.e. about 240 μm. In the second zone, corresponding to unimplanted material, the fracture mode is fully ductile, as expected for T91

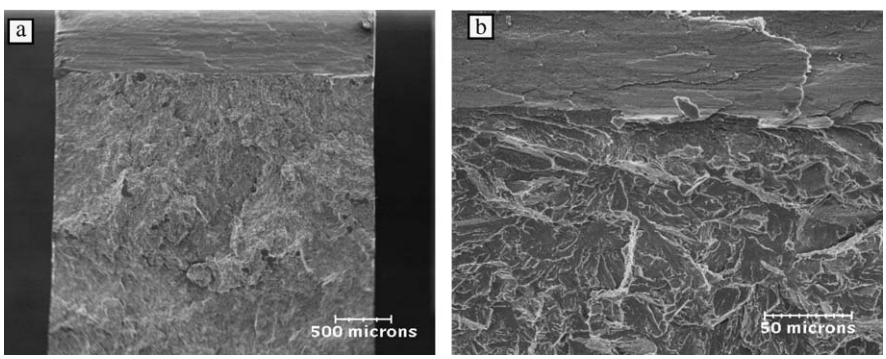

Fig. 6. SEM micrographs showing the fracture surface of a T91 specimen following three-point bending test at −170 °C: (a) general fracture appearance and (b) zoom in the failure initiation zone close to the notch root.

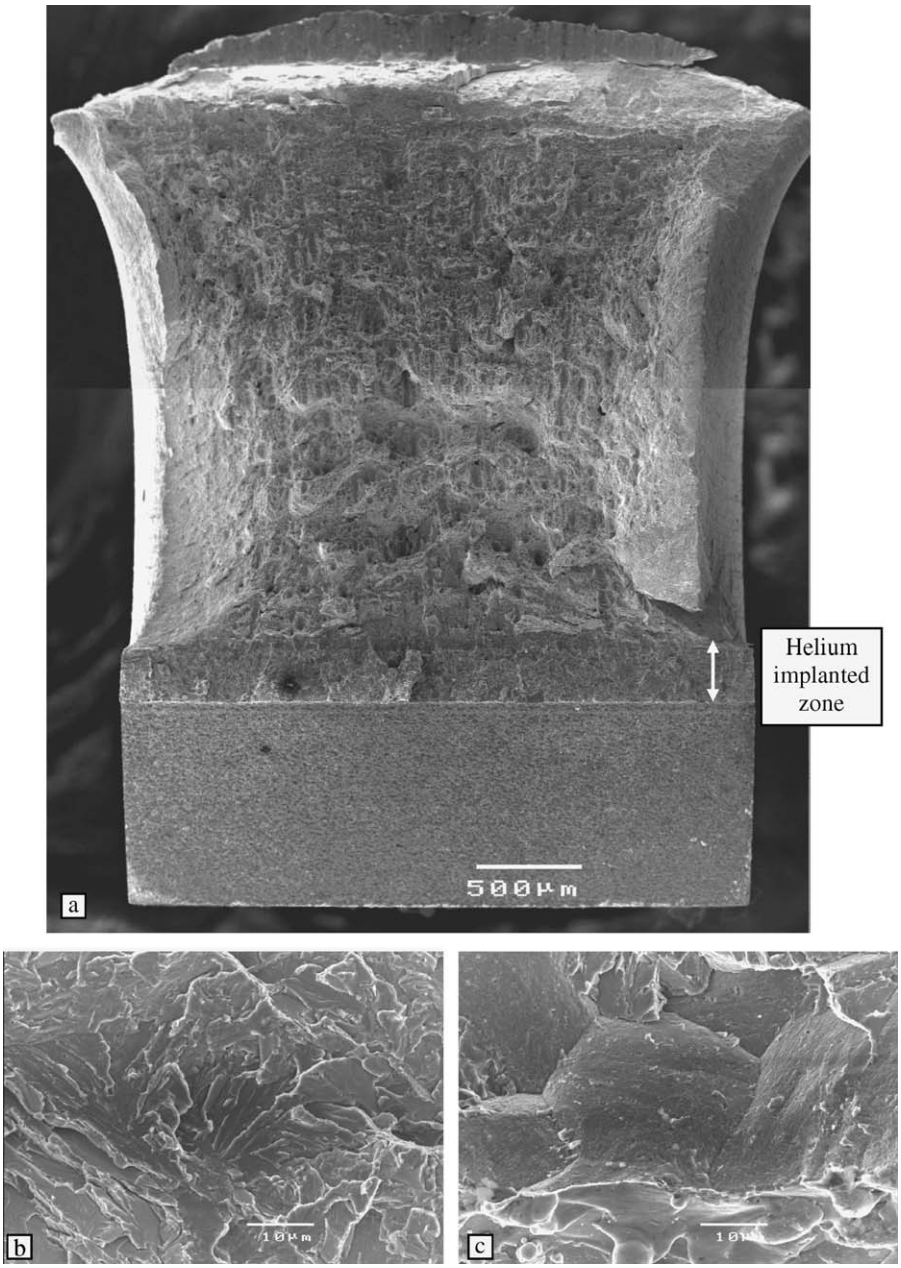

Fig. 8. SEM micrographs showing the fracture surface of a T91 specimen implanted with 0.25 at.% helium following three-point bending test at room temperature: (a) general view of the broken specimen and (b, c) details of the fracture surface in the brittle, helium implanted zone.

submitted to static bending tests at room temperature.

3.3. Mechanical analysis of the tests

3D finite elements calculations of the bending tests were carried out in order to obtain the local strain and stress fields. In the case of unimplanted T91, this was done using as input data the constitutive behaviour deduced from tensile tests performed at −170 °C on cylindrical specimens. The applied load as a function of opening displacement was calculated and good agreement with experimental data was found, as shown in Fig. 9. In the case of

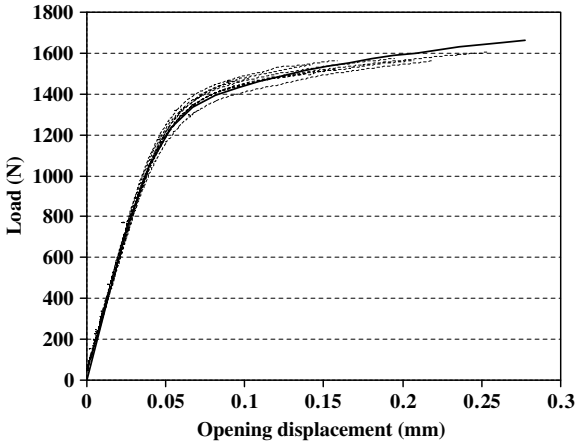

Fig. 9. Applied load as a function of opening displacement for T91 tested in three-point bending at 170 °C. Experimental bending curves (dotted lines) are plotted together with the results of 3D FE calculations (solid line).

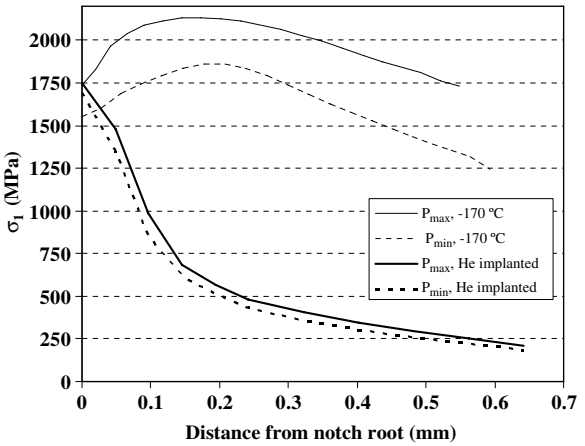

Fig. 11. Evolution of the maximum principal stress σ_1 as a function of the distance to the notch root. In the labels, P_{max} (respectively P_{min}) indicate the curves which correspond to the highest (respectively lowest) opening displacement at failure (or at the onset of 'pop-in' crack propagation).

helium implanted samples, FE calculations were performed using two constitutive behaviours: one for unimplanted T91, the other for T91 charged with helium, which was derived from the results of the tensile tests carried out on helium implanted specimens [3]. Again, there is good agreement between the calculated and experimental curves (see Fig. 10) up to the load at which the 'pop-in' occurred.

The values of the maximum principal stress σ_1 as a function of distance to the notch root were calculated and are presented in Fig. 11 both for pristine and implanted T91. In each case, two curves are plotted: they represent the σ_1 evolution for an opening displacement equal to the highest, respectively lowest, value at failure (or at the onset of the 'pop-in') measured experimentally. Likewise, for these four cases, the ratio of the equivalent Von Mises stress to the yield stress is plotted in Fig. 12. This ratio gives a qualitative indication of the local amount of plastic deformation.

Fig. 11 shows that significantly higher σ_1 values were reached in the unimplanted samples tested in the brittle domain compared to the case of helium

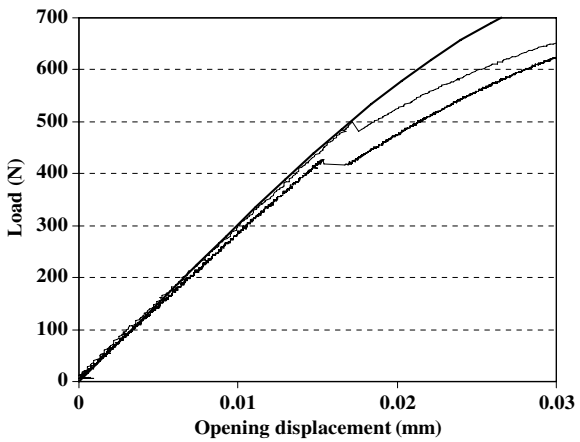

Fig. 10. Applied load as a function of opening displacement for He implanted T91 tested in three-point bending at room temperature. Two experimental bending curves (fine lines) are plotted together with the results of 3D FE calculations (heavy line).

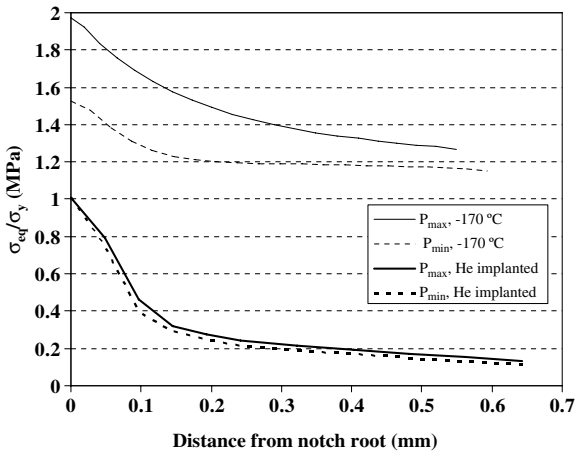

Fig. 12. Evolution of the ratio equivalent Von Mises stress to the yield stress as a function of the distance to the notch root. In the labels, P_{max} (respectively P_{min}) indicate the curves which correspond to the highest (respectively lowest) opening displacement at failure (or at the onset of 'pop-in' crack propagation).

implanted samples tested at room temperature. These high stress values extend over a large distance from the notch root whereas in implanted samples σ_1 quickly drops with increasing distance from the notch. Also, in unimplanted specimens, a large volume of material experienced plastic deformation before failure, as shown in Fig. 12. By contrast, there was very little plastic deformation in helium implanted specimens when 'pop-in' crack propagation was triggered.

4. Discussion

The experiments performed in this study clearly show a drastic embrittlement of T91 by the implanted helium. This is a typical case of 'Non-hardening embrittlement' [5], as it does not only result from the hardening due to implantation. Indeed, helium induces a reduction in the critical stress for brittle fracture, since, for the same sample geometry, brittle fracture occurred in the implanted zones for values of the maximum principal stress below 1750 MPa, whereas at failure, the highest values of σ_1 were in the range 1850–2150 MPa for the unimplanted samples tested at −170 °C. Obviously, the implanted helium lowers the grain boundary cohesion as a significant amount of intergranular areas were observed on the fracture surfaces of the samples containing helium while the fracture appearance was almost fully cleavage in the unimplanted case.

The mechanical analysis of the experimental data thus indicate that 0.25 at.% helium implanted at 250 °C causes T91 to become more brittle at room temperature than in the unimplanted condition at −170 °C. In order to go further in our analysis, we have attempted to evaluate the fracture toughness of T91 loaded with helium using the Beremin model of brittle fracture [11]. It must be stressed that this is very tentative, since the model assumes that some plastic deformation of the sample occurs before brittle failure is triggered. As pointed out in Section 3.3, FE calculations showed that there was very little plastic deformation in the implanted zones before the onset of 'pop-in' fracture.

In the following, we will first model the fracture properties of pristine T91 in the brittle domain using the Beremin approach, as this has never been done previously. The method will then be applied to the case of implanted T91.

In the Beremin model, it is assumed that plastic deformation induces the formation of microcracks at microstructural features like carbides. If locally the maximum principal stress σ_1 reaches a critical value, which depends on the microcrack size, unstable fracture occurs. Assuming a power law for the microcracks size distribution, the failure probability $p_r(\sigma_1)$ for a volume V_0, where the stress level is σ_1, is given by

$$p_r(\sigma_1) = 1 - \exp\left(-\left(\frac{\sigma_1}{\sigma_u}\right)^m\right), \tag{7}$$

where m and σ_u are material constants which characterize the fracture behaviour of the steel. The parameter m describes the scatter in the microcrack size distribution, while σ_u is related to the intrinsic cleavage stress of the material.

Using the weakest-link assumption, the failure probability for the whole specimen, P_R is given by

$$P_R = 1 - \exp\left(-\left(\frac{\sigma_w}{\sigma_u}\right)^m\right), \tag{8}$$

$$\text{where } \sigma_w = \left[\int_{V_p} \sigma_1^m \frac{dV}{V_0}\right]^{1/m} \tag{9}$$

is the Weibull stress and V_p the plastically deformed volume. As in [11], V_0 was chosen as 50 μm^3.

The values of the material parameters m and σ_u were determined based on the results of the bending tests, by fitting the calculated failure probability to the experimental data using the maximum likelihood method [12]. The optimum values for m and σ_u are reported in Table 2. The experimental and calculated failure probabilities are plotted in Fig. 13.

Once the values of the material parameters are obtained, the Weibull stress and hence the failure probability can be computed by FE simulations for a given mechanical test and specimen geometry. In the present case, this was done for a toughness test performed on CT specimens. In Fig. 14, the experimental failure probability is plotted together with model predictions. The agreement between model results and experiment is quite good, given

Table 2
Values of the fracture parameters as defined in the Beremin model, identified using static bending tests at −170 °C

m	m^-	m^+	σ_u (MPa)	σ_u^- (MPa)	σ_u^+ (MPa)
13.5	7.4	19.2	3380	3206	3565

Confidence intervals $(m^-, m^+; \sigma_u^-, \sigma_u^+)$ corresponding to a confidence level of 95% are indicated as well.

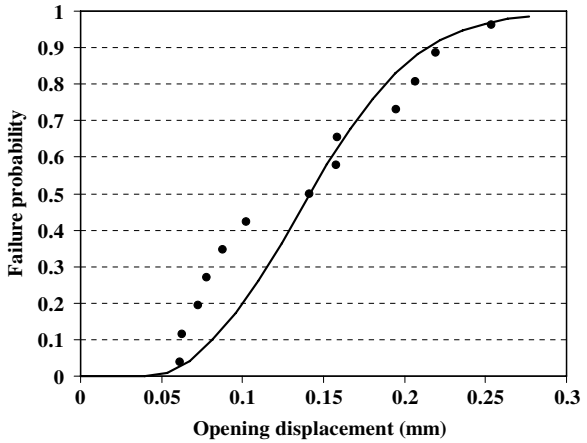

Fig. 13. Experimental (dots) and calculated (continuous line) failure probabilities as a function of opening displacement for T91 tested in three-point bending at −170 °C.

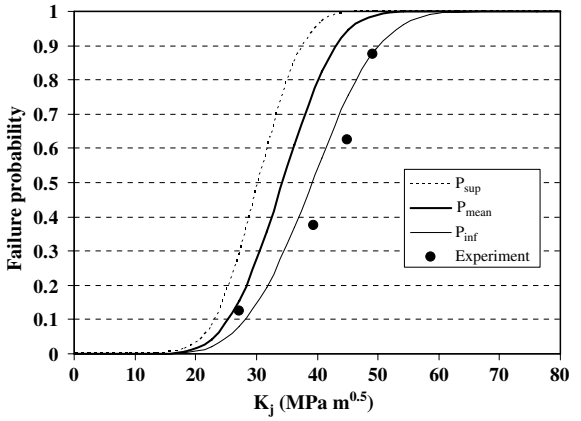

Fig. 14. Experimental and calculated failure probabilities as a function of stress intensity factor for T91 CT specimens tested at −170 °C. P_{sup} and P_{inf} correspond to curves calculated using (m, σ_u^+) respectively (m, σ_u^-) values reported in Table 2. P_{mean} was calculated using the optimum values (m, σ_u).

the fact the experimental probability was derived based on the results of only four tests.

We have then attempted to model the fracture properties at room temperature of helium implanted T91 using the same approach. The fact that helium loading was restricted to a shallow zone around the notch, does not prevent from implementing the method, as brittle fracture was triggered within the implanted zone. The experimental values for the opening displacements at failure were set equal to those at which the 'pop-in' occurred. The parameters m and σ_u which characterize the fracture properties at room temperature of helium implanted T91 were then obtained using the fitting procedure described above and are given in Table 3. In addition, calculated and experimental failure probabilities are plotted in Fig. 15.

Table 3
Values of the fracture parameters for helium implanted T91 as defined in the Beremin model, identified using static bending tests at room temperature

m	m^-	m^+	σ_u (MPa)	σ_u^- (MPa)	σ_u^+ (MPa)
31.6	10.3	50.7	1870	1795	1954

Confidence intervals ($m^-, m^+; \sigma_u^-, \sigma_u^+$) corresponding to a confidence level of 95% are indicated as well.

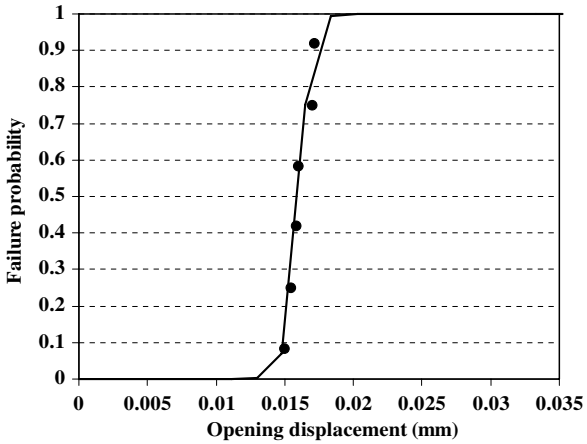

Fig. 15. Experimental (dots) and calculated (continuous line) failure probabilities as a function of opening displacement for helium implanted T91 tested in three-point bending at room temperature.

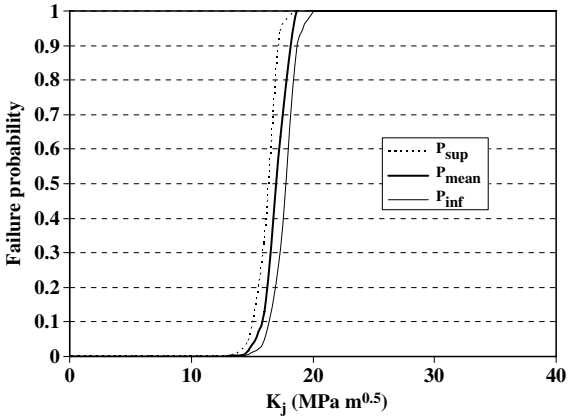

Fig. 16. Calculated failure probabilities as a function of stress intensity factor for a toughness test at room temperature on helium implanted T91. P_{sup} and P_{inf} correspond to curves calculated using (m, σ_u^+) respectively (m, σ_u^-) values reported in Table 3. P_{mean} was calculated using the optimum values (m, σ_u).

Finally, the model was used to predict the toughness at room temperature of T91 loaded with 0.25% at He at 250 °C. Calculated failure probabilities as a function of the stress intensity factor are presented in Fig. 16. The predicted mean fracture toughness at room temperature following helium implantation is 17 MPa $m^{1/2}$, whereas at −170 °C the measured toughness of pristine T91 was found to be about 35 MPa $m^{1/2}$.

5. Summary/conclusion

Static bending tests were carried out at room temperature on T91 miniature Charpy specimens implanted at 250 °C in the notch with 0.25 at.% helium. For comparison purposes, tests were also performed on unimplanted samples at −170 °C, i.e. in the brittle fracture domain. 'Pop-in' phenomena were systematically observed for the six implanted specimens and SEM observations revealed a fully brittle fracture appearance in the implanted zones, with both transgranular cleavage and intergranular fracture. By contrast, for unimplanted samples tested at low temperature, the fracture mode was cleavage. In addition, FE showed that brittle fracture occurred in the implanted samples at lower σ_1 values than in the case of unimplanted samples. Both the FE analysis and the SEM observations demonstrate that the implanted helium has induced a decrease in the critical stress for intergranular fracture. Indeed, the Beremin model, which was tentatively applied, predicts a lower fracture toughness at room temperature for T91 charged with 0.25 at.% helium than that measured at −170 °C for the unimplanted steel. As this work has shown the relevance of the chosen experimental approach to investigate helium effects on the fracture properties of T91 steel, additional tests will be carried out on samples implanted at lower helium concentrations and/or at different implantation temperatures.

References

[1] G.S. Bauer, M. Salvatores, G. Heusener, J. Nucl. Mater. 296 (2001) 17.
[2] H. Schroeder, H. Ullmaier, J. Nucl. Mater. 179–181 (1991) 118.
[3] P. Jung, J. Henry, J. Chen, J.-C. Brachet, J. Nucl. Mater. 318 (2003) 241.
[4] J. Henry, M.-H. Mathon, P. Jung, J. Nucl. Mater. 318 (2003) 249.
[5] G.R. Odette, T. Yamamoto, H. Kishimoto, Fusion materials semiannual report, 2004.
[6] R. Klueh, D. Harries, High-Chromium Ferritic and Martensitic Steels for Nuclear Applications ASTM Monograph, MONO3, 2001, p. 156.
[7] R. Lindau, A. Möslang, D. Preininger, M. Rieth, H.D. Röhrig, J. Nucl. Mater. 271–272 (1999) 450.
[8] R. Kasada, T. Morimura, A. Hasegawa, A. Kimura, J. Nucl. Mater. 299 (2001) 83.
[9] Y. Dai, X. Jia, K. Farrell, J. Nucl. Mater. 318 (2003) 192.
[10] X. Jia, Y. Dai, J. Nucl. Mater. 323 (2003) 360.
[11] F.M. Beremin, Met. Trans. 14A (1983) 2277.
[12] ESIS Procedure P6-94: Draft procedure to measure and calculate material parameters for the local approach to fracture using notched tensile specimens.